Surface curvature and aminated side-chain partitioning affect structure of poly(oxonorbornenes) attached to planar surfaces and nanoparticles of gold

Ali Rahnamoun,† Alyssa Deline,† Joanna Zienkiewicz,† Ronghua Bei,† Zheng Zheng,‡ Zeev Rosenzweig,‡ Howard Fairbrother† and Rigoberto Hernandez†,*

†Department of Chemistry, Johns Hopkins University, Baltimore, Maryland 21218, United States
‡Department of Chemistry and Biochemistry, University of Maryland Baltimore County, Baltimore, Maryland 21250, United States

Abstract

Cationic amphiphilic polymers are often used to coat nanoparticles as they increase chemical stability in solution, and exhibit membrane disruption activities. Among these, poly (oxonorbornenes) (PONs) are tunable membrane disruptors. They can be constructed with either one amine-terminated side chain and one hydrophobic alkyl side chain (PON-50) or two amine-terminated side chains (PON-100) on each repeat unit, and can then be conjugated to gold nanoparticles using O-(2-carboxyethyl)-O′-(2-mercaptoethyl) heptaethylene glycol (HEG) spacers. While the amine content and membrane disruption activity of PONs can be controlled, the detailed structural properties of PONs conjugated to gold nanoparticles remain less understood. To address this, we performed molecular dynamics simulations of PON-50 and PON-100 to determine the non-bonded energies of PONs structures as a function of amine composition. We found increasing energetic stabilization with decreasing amine composition. These results were consistent with experimental observations obtained with X-ray photoelectron spectroscopy (XPS) in which PON-100 was found to have the lowest conjugation efficiency to gold surfaces out of a range of PONs amination ratios. Computationally obtained energetics suggest that replacing the aliphatic amine groups with aromatic amine groups can reverse this behavior and lead to more stable PONs structures with increasing amine content. We also found that the curvature of the gold nanoparticle surface affects interactions between the surface and

the amine groups.of PON-50. Increasing curvature decreased these interactions, resulting in a smaller effective footprint of the HEG-PON-50 structure.

Introduction

The use of engineered nanoparticles (ENPs) in commercial and industrial applications continues to grow exponentially.[1-3] As the production increases, it becomes increasingly important to consider the extent to which given types of ENPs are sustainable or have the potential to exhibit deleterious environmental effects. This suggests a prioritization for the characterization and prediction of the properties of those ENPs which are targeted for production.[4-5] For example, the surface of an ENP is often modified with surface functional groups in order to control their behavior during the different stages of production, processing, and final application[6-11] One such class of ENPs includes nanoparticles that are attached to synthetic polymers as they have been seen to lead to promising improvements in therapeutic performance,[12-14] and are accessible to all-atom and coarse-grained molecular dynamics techniques.[15] Cationic polymer coatings serve as the primary interface between ENPs and biological membranes in cells and organisms. Indeed, the choice and structure of these coatings are critical to determining and designing the resulting biological interactions and toxicity of ENPs.[16-22]

Several groups have found that gold nanoparticles (AuNPs) functionalized with positively charged polymers lead to significantly more bacterial selectivity than AuNPs functionalized with anionic polymers.[9, 23-25] Klaper and colleagues found that AuNPs functionalized with two cationic polymers, poly(allylamine hydrochloride) (PAH) and hexadecyltrimethyl ammonium bromide (CTAB), were orders of magnitude more toxic than negatively charged particles and had significant effects on the mortality of the water flea *Daphnia magna* at concentrations as low as 10μg L^{-1}.[9] Another study by Parak et al. showed that both cellular uptake and cytotoxicity was increased for AuNPs coated with cationic amphiphilic polymers when compared to their anionic counterparts.[26] Such findings could be anticipated from the fact that many cationic polymers have been seen to be toxic to eukaryotes. Clustering them on a surface increases their local concentration and should thus also enhance any toxic effects. In addition to charge, the relative hydrophobicity of polymer coatings also has significant impact on the membrane disruption activity, and resulting bacterial selectivity, of ENPs.[27-28] Amphiphilic polymers in particular are known to exhibit high antibacterial activity and increased disruption of lipid membranes.[23, 29]

One promising class of cationic, amphiphilic polymeric coatings is poly(oxonorbornenes) (PONs), which have been tuned in the absence of ENPs to achieve highly selective bioactivity to both specific cell types (i.e. bacterial versus mammalian cells) and bacterial types (i.e. Gram-positive versus Gram-negative bacteria).[30] It is therefore possible to synthesize highly selective, antimicrobial and non-hemolytic macromolecules by adjusting the charge distribution and local exposed hydrophobicity of cationic amphiphilic polymers, allowing for enhanced antimicrobial activity without the risk of unintended toxicity to other organisms. PONs can be conjugated to nanoparticle surfaces using 1-ethyl-3-(3-dimethylaminopropyl) carbodiimide (EDC) coupling to modify O-(2-carboxyethyl)-O′-(2-mercaptoethyl) heptaethylene glycols (HEGs) that are covalently bonded to the nanoparticle surface (HEG-PONs).[31]

Because PONs are built from a modular synthesis platform,[30] their hydrophobic/hydrophilic balance can be modified by synthesizing PONs with either one charged amine-terminated side chain and one hydrophobic alkyl side chain (PON-50) or two amine-

terminated side chains on each repeat unit (PON-100), as well as intermediate amine contents. Previous studies in the Rosenzweig and Lienkamp groups have shown that PON-50 with 50% aliphatic amine terminal groups and 50% alkyl groups exhibit greater membrane disruption activities than PON-100 with 100% aliphatic amine terminal groups.[30-31] Zheng *et al*[31] used PONs as a model polymeric ligand to investigate how amine content impacts the strength of PONs-AuNP interactions with unilamellar liposomes. They found that PONs-AuNPs with high PONs surface coverage had membrane disruption activities that were an order of magnitude greater than the equivalent free PONs, and attributed this enhanced activity to the localized pockets of high ammonium ion concentration provided by AuNPs. While increasing amine content should increase membrane disruption in the absence of any other changes, it was instead found that an increase in the percent of amine side chains in the PONs from 50% to higher composition—viz, 55%, 75%, 95%, and 100%—resulted in a systematic decrease in liposome lysis efficiency because they were replacing alkyl groups that are even more disruptive. They also found that PON-50 exhibited higher conjugation efficiency to AuNPs and were able to bind to the surface through a covalent attachment at a single point, leaving the polymer chains pointing directly outward. In contrast, PON-100 tended to collapse onto the AuNP surface, suggesting that PON-50 are more stable, although alternative interpretations cannot be entirely ruled out.[31] Therefore, it is not just the amine content but the stability and orientation of the PONs ligands that control the membrane disruption activity of PONs-AuNPs.

The goal of this work is to reveal how amine density and structure affects the properties of PONs, which can in turn give further insight into the behavior and environmental impact of PONs-coated ENPs. We use a computational approach to determine the relative energetics of various cationic PONs and benchmark it with experiment. In examining the effect of the curvature of the Au surface on the structure of a single HEG-PON ligand, we find that the AuNP size can play a role in the effective surface coverage of PONs. We also perform a statistical analysis of the interaction energies of PONs of varying amine composition and structure by sampling structures obtained from molecular dynamics simulations. Our findings of the energetics reveal a possible molecular-scale explanation of the reported trends in the effects of PON amine composition. In particular, we find consistent trends between favorable energetics of adjacent PON molecules to their experimentally observed properties such as their coverage on Au surfaces.

METHODS

HEG-PON conformations on Au surfaces with varying curvature

The structures of a single HEG-PON ligand on a planar gold surface and on gold nanoparticles with different surface curvatures were determined through molecular dynamics simulations. Specifically, models of single HEG-PON on gold nanoparticles of varying size were simulated and contrasted to the limiting case of a planar gold surface. That is, three different cases were investigated: (1) HEG-PON-50 on a tile of a planar gold surface satisfying periodic boundary conditions; (2) HEG-PON-50 on a section of a 32 nm diameter gold nanoparticle, and (3) HEG-PON-50 on a 4 nm diameter gold nanoparticle. The corresponding initial configurations

of these models are shown in Fig. 1. Here, we assumed a single connection point as suggested by the PON-50 experiments,[31] and allowed the system to relax so as to determine the degree of collapse without imposing additional connection points.

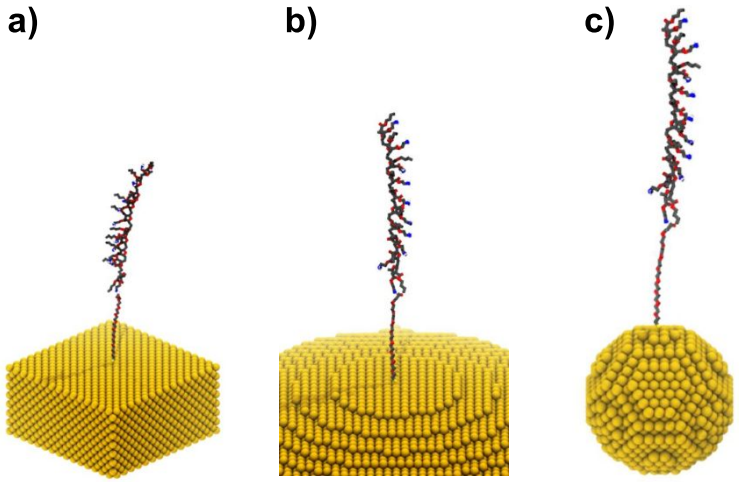

Figure 1. Initial configurations of HEG-PON-50 on gold: (a) a planar gold surface, (b) a periodic tile of a portion of a 32nm gold nanoparticle, and (c) 4 nm gold nanoparticle.

Simulations of various HEG-PONs on gold surfaces structured as indicated in Fig. 1 were performed using the LAMMPS molecular dynamics simulation package.[32] The OPLS force field was used to describe the energetics of the HEG-PON-50 ligand which includes ten PON-50 repeat units attached to one HEG. Water molecules were modeled using the TIP3P model and the Gold atom interactions in the gold nanoparticle were modeled using Lennard-Jones potentials. The solvated configurations were equilibrated first in the *NVT* ensemble (with constant number of atoms, volume and temperature) at 294 K for 1.5 ns while the HEG-PON molecule atoms positions were constrained so as to relax the solvent, and then in the *NPT* ensemble at 1 atm and 294 K for an additional 5.5 ns so as to relax the solvated HEG-PON. At the end of the equilibrations, the projected areas of the HEG-PON-50 ligand on the gold surfaces were calculated as a measure of the effects of gold surface curvature on the configurations of these ligands.

Statistical analysis of the interaction energies

The structures of the previously synthesized and reported[31] PON-50 and PON-100 repeat units are shown in Fig. 2. These can be modeled as having either neutral or charged amine terminal groups. In addition to these aliphatic amine terminal groups, we also modeled the energetics of hypothetical PON-50 and PON-100 structures containing neutral and charged aromatic amine terminal groups. These hypothetical PONs structures are shown in Fig. 3. We used molecular dynamics simulations with an explicit solvent to determine the interaction energies of PONs with different contents of aliphatic amine, charged aliphatic amine, aromatic amine or charged aromatic amine terminal groups.

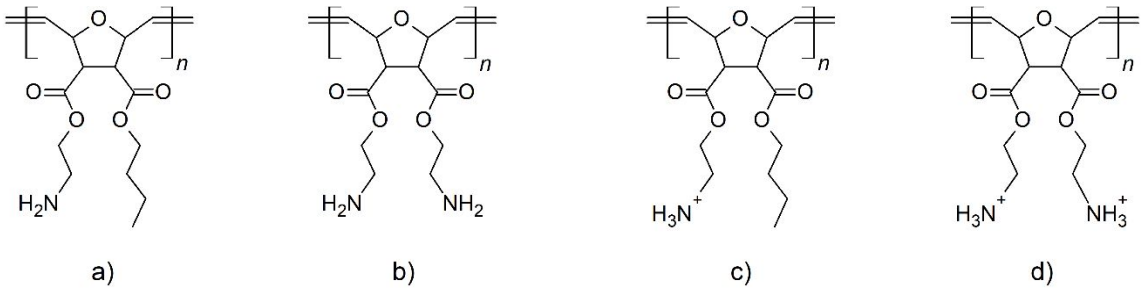

Figure 2. PON molecules with (a) 50% aliphatic amine content, (b) 100% aliphatic amine content. (c) 50% charged aliphatic amine content, and (d) 100% charged aliphatic amine content.

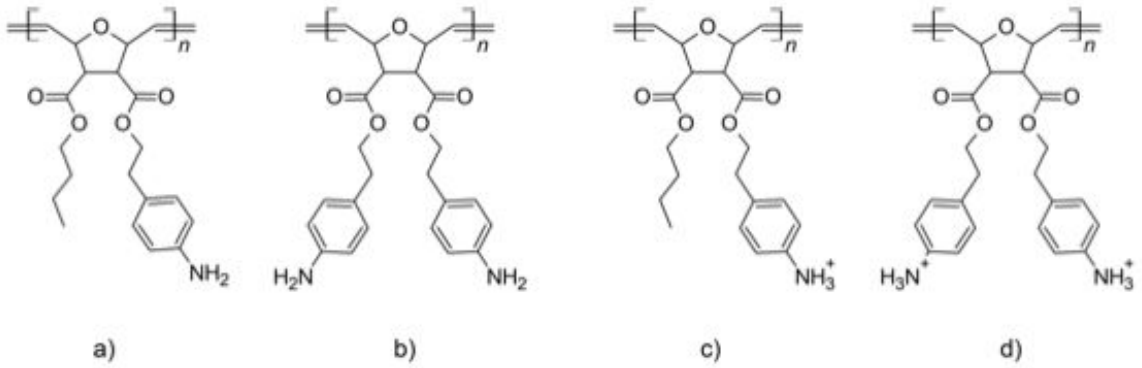

Figure 3. PON molecules with (a) 50% aromatic amine content, (b) 100% aromatic amine content. (c) 50% charged aromatic amine content, and (d) 100% charged aromatic amine content.

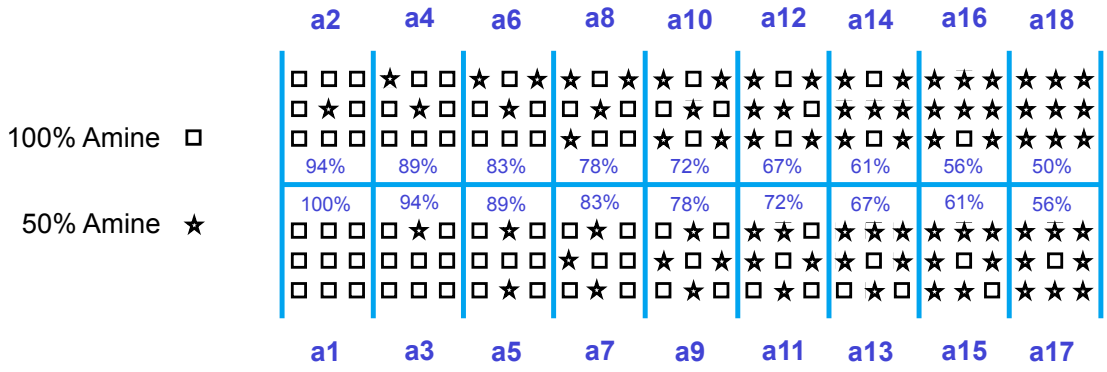

Figure 4. The eighteen initial rectilinear configurations for the placement of PON-50 and PON-100 molecules within a periodic tile as employed in the simulations. The star represents PON-50, the square represents PON-100, and the overall amine content is noted by the corresponding percentage.

Simulations were performed using the commonly-available package NAMD—nanoscalable molecular dynamics.[33] All structures were described with the CHARMM general force field and water molecules were modeled using the TIP3P model. The parameters for PON-

50 and PON-100, were generated by analogy using the CHARMM General Force Field (CGenFF) program.[34] The choice of a different force field for this set of calculations than that used in the gold-ligand simulations was made because of the relative convenience for each calculation with regards to ease of implementation in the corresponding programs. This should not lead to inconsistencies as the differences between the two selected force fields are expected to be relatively small, as recently reported,[35]

Each PON-50 or PON-100 molecule modeled in the simulations includes 6 repeat units. They consisted of configurations constructed of different combinations of nine molecules on a periodic tile, placing adjacent ligands 10 Å apart in rectilinear configuration composed of PON-50 or PON-100 (Fig. 4), This distance (and corresponding surface attachment density) was chosen because it was large enough that the uncoiled chains were not initially overlapping, but small enough that the chains interacted as they relaxed. The resulting systems were either net neutral requiring no addition of counterions, or had a net positive charge which was neutralized with the appropriate equivalent of chlorine ions. Solvated configurations were energy minimized and then equilibrated in the *NPT* ensemble (with constant number of atoms, pressure and temperature) at 1 atm and 294 K for a total of 3 ns while removing the harmonic constraints on the solvated molecules sequentially. Parallelepiped simulation boxes with periodic boundary conditions were used in every simulation. The choice of a tile with only 9 PONs molecules was made as a compromise between the computational cost of the simulations and subsequent non-bonded interaction energy calculations, and the need to consider a (minimal) system large enough to have uncorrelated interactions. The selected partitions, enumerated in Fig. 4, lead to a variable amine composition as noted therein, and which ranges from 50% to 100%, and variations in their relative arrangements. A representative snapshot of an equilibrated structure of an all-PON-50 simulation (corresponding to a18 of Fig. 4) is shown in Fig. 5.

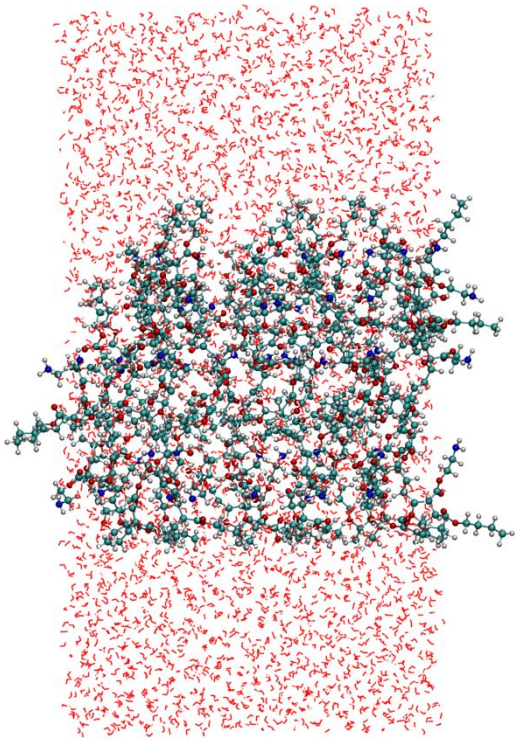

Figure 5. A representative equilibrated structure of an all PON-50 with aliphatic amine terminal groups in a bilayer exposed to water in a periodic box corresponding to the tiling of case a18 in Fig. 4.

Experimental evaluation of HEG-PONs coverages on flat, polycrystalline Au surfaces

The synthesis and purification of PONs ligands with aliphatic side chains, and their conjugation to Au surfaces via EDC coupling to HEG, were performed as previously described.[30-31, 36] The resulting PON molecule is is attached to the HEG spacer through an EDC coupling, and the HEG spacer is attached to the gold surface through a thiol bond.[37] X-ray photoelectron spectroscopy (XPS) was used to probe the PONs coverage on flat, polycrystalline Au surfaces. A range of PONs amine/alkyl side chain ratios was tested, including 50, 55, 75, 95, and 100% aminated PONs. The structures of 50%, 75%, and 100% aminated PONs are shown in Fig. 6. Au substrates were prepared by dicing an aluminosilicate glass microscope slide coated with a 1000 Å layer of Au (Asemblon, Redmond, WA) into 1 cm^2 squares. The substrates were sputter-cleaned with argon ions to remove carbon contamination using a PHI 04-303 Differential Ion Gun in a PHI 5600 XPS system.

Once cleaned, each substrate was removed from vacuum and immediately transferred into a 50 mL glass crystallization dish containing 20 mL of distilled deionized (DDI) water and 300 µL of 21.8 mM HEG spacer. The solution was covered with a glass petri dish and substrates were permitted to react with the HEG spacer overnight. Substrates were then thoroughly rinsed with DDI water to remove unreacted HEG. Two HEG-Au samples were then immediately placed on the sample stub with copper clips and introduced into the XPS ultra-high vacuum (UHV) chamber for storage until analysis. The remaining HEG-Au substrates were placed into individual 50 mL glass crystallization dishes containing 20 mL of 10 mM 4-(2-Hydroxyethyl)piperazine-1-ethanesulfonic acid (HEPES) buffer at pH 6.0, 200 µL of 50 mM *N*-hydroxysulfosuccinimide sodium salt (Sulfo-NHS), 100 µL of 50 mM EDC, and 200 µL of 3.3 mM PONs with one of the chosen amine/alkyl ratios. Each dish was covered with a glass petri dish and permitted to react for 4 h, after which each substrate was thoroughly rinsed with HEPES, then DDI water. Each substrate was then placed on a sample stub with copper clips, introduced into the UHV chamber, and analyzed.

XPS analysis was performed on a PHI 5600 XPS system equipped with a Mg Kα flood source (1253.5 eV) and a hemispherical energy analyzer at a base pressure of 10^{-9} Torr. Survey scans were collected at a pass energy of 187.85 eV with a 1.6 eV/step size and 5 sweeps. High resolution multiplex scans of C 1s, O 1s, N 1s, and Au 4f regions were collected at a pass energy of 58.7 eV with a 0.125 eV/step size and 20 sweeps. All XPS data were analyzed using CasaXPS software.

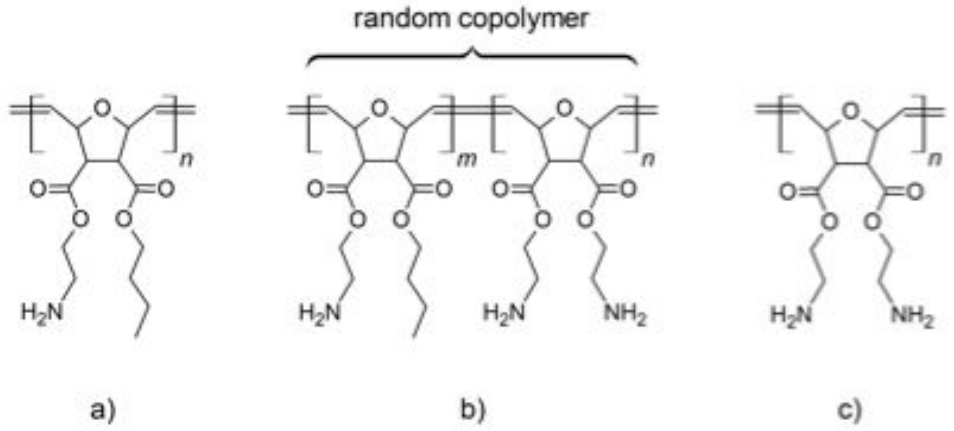

Figure 6. Example structures of PONs molecules investigated in experimental evaluation of HEG-PONs coverages of Au. They are constructed using oxonorbornene monomers with varying amination in the two side chains: (a) 100% of the monomers in PON-50 each have one alkyl and one amine side chain; hence, they are 50% aminated, (c) 100% of the monomers in PON-100 have two amine side chains; hence they are 100% aminated. (b) PON-*x* with $x=100*(m+2n)/(2m+2n)$, is constructed using a random copolymer of *m* and *n* monomers, as indicated, such that *x*% of all the side chains are aminated. For example, in PON-75, $m=n$ and 50% of the monomers have both chains aminated.

Results

HEG-PON conformation on gold surfaces with varying curvature

Ligand equilibrations on a planar gold surface and gold nanoparticles with 4 nm and 32 nm radii were performed to obtain characteristic configurations of the ligands so as to estimate the effect of gold surface curvature on the configuration of the HEG-PON ligand. Surface coverages of the HEG-PON ligand attached to the above-mentioned gold surface cases by thiol linkages were measured at the end of equilibration to quantify the degree of collapse of the structure of the HEG-PON ligand. Example configurations of HEG-PON ligands on planar gold surfaces and gold nanoparticles at the end of equilibrations are shown in Fig. 7. The projected area of the HEG-PON ligand on the surface serves as a measure of surface coverage. These projected areas are shown in Fig. 8. To determine whether the ligand stays in the solution or collapses on the surface, the number of amine groups collapsing within 0.7 nm (more than twice the water molecule diameter) of the surface are tracked during the equilibrations (Fig. 9).

Our results suggest that curvature of the gold surface affects the HEG-PON ligand's configuration on the surface. HEG-PONs collapse more readily onto a planar gold surface and gold NPs with smaller curvature than for NPs with larger curvature. We find that between 6 to 8 amine groups collapse onto the 32 nm gold nanoparticle. This is also consistent with the projected area analysis. The HEG-PON ligand covers a larger projected area on gold surface with little or no curvature—viz, the planar surface. Specifically, we found that the average area of the footprint on the planar surface is about 13 nm^2, which corresponds to an effective diameter of 4 nm. Such an area is comparable to that of the two-dimensional cross-section of a 4nm NP, and hence the contraction to a smaller footprint (at 7.4 nm^2) is to be expected when the curvature is increased

to represent a 4 nm NP. These values are, of course, the expected diameters in the limit of a single HEG-PONs attached to the surface. In order to observe interactions between the HEG-PONs on the planar surface, their density must therefore be high enough that the mean distance between the chains is less than 4nm while being greater than the width of a single monomer. The distance of 1 nm (= 10 Å) between the chains employed in the simulations of the assemblies in the next subsection is consistent with this range.

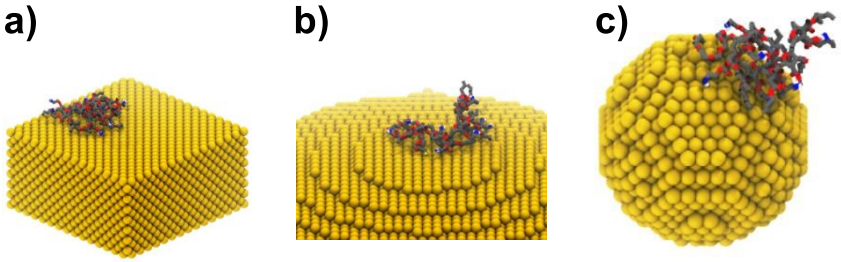

Figure 7. Configurations of HEG-PON ligands on a planar gold surface and gold nanoparticles at the end of equilibrations for a (a) planar surface, (b) a portion of a 32nm NP, and (c) a 4nm NP.

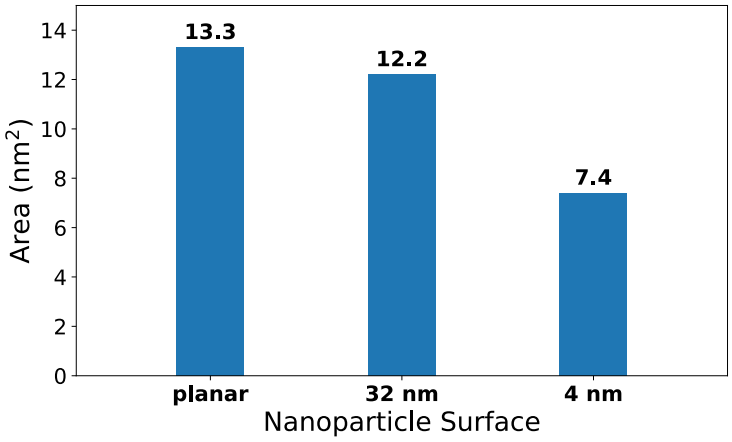

Figure 8. Surface Coverage per HEG-PON Ligand calculated as projected area of the ligand on the surface (nm^2).

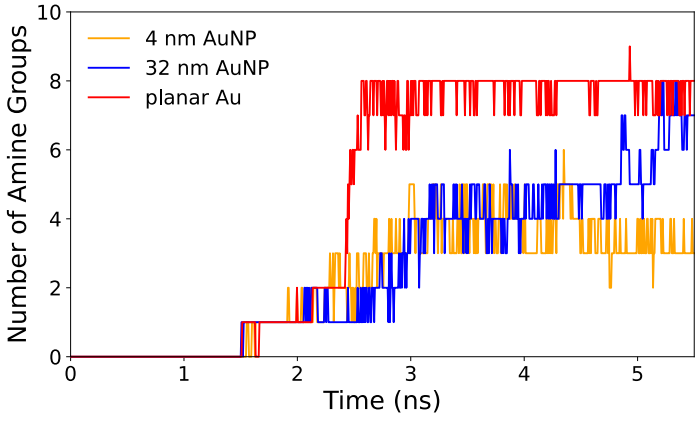

Figure 9. Number of amine groups (out of 10) collapsing onto the surface. The number of amine groups collapsing within 0.7 nm of the surface are calculated during the equilibrations.

Statistical analysis of the interaction energies

The average interaction energies between the chains of PONs assemblies with varying composition and arrangements were obtained by molecular dynamics simulations as described in the Methods. Once equilibrated, the last 0.1 ns of each simulation was recorded and used for the calculation of the reported observables such as the non-bonded interactions between the chains. The interactions between atoms which are not linked by covalent bonds include electrostatic and Van der Waals interactions. The average non-bonded energies between chains calculated for the 18 different model configurations of Fig. 4—varying the distribution and positions of PON-50 and PON-100—are shown in the top panel of Fig. 10. The related change in these energies relative to the maximum value for a given amine are shown in the bottom panel of Fig. 10. We find that the models including all PON-50 molecules with aliphatic amine terminal groups show more stability than the models including all PON-100 molecules. Both this finding and previous experimental results related to PONs surface coverage and resultant ζ-potentials[31] are consistent with the interpretation that PON-50 binds to the surface at a single point leaving the ligand pointing outward, while PON-100 tends to collapse onto the surface. We also find that replacing the aliphatic amine groups with aromatic amine groups can reverse this behavior leading to more stable assemblies when they contain a higher percentage of PON-100 molecules. These results also suggest that for the models constructed with charged terminal groups, the mixture of PON-50 and PON-100 introduces more stable assemblies than those with 100% PON-50 composition.

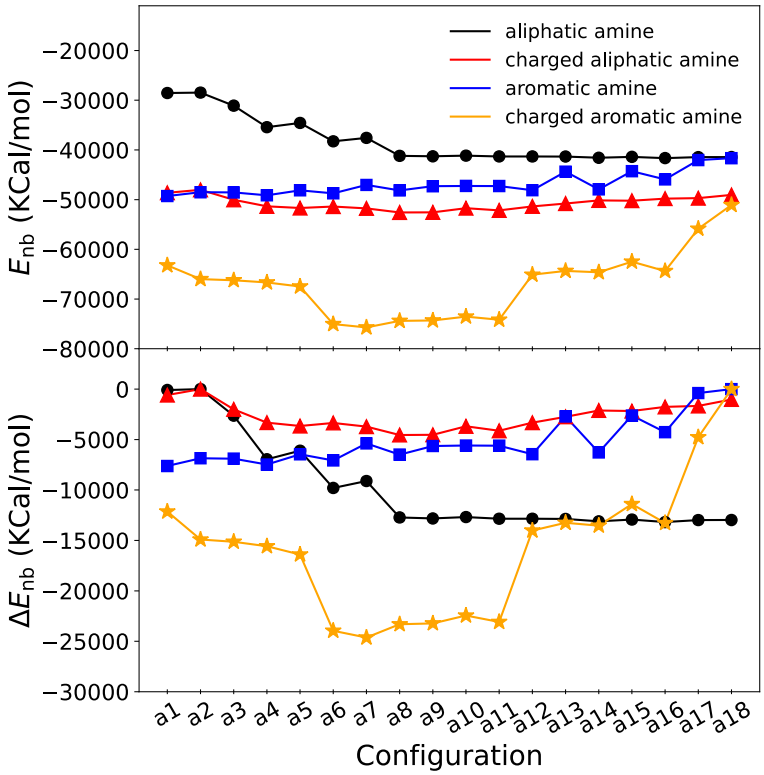

Figure 10. Average non-bonded energies E_{nb} (top panel) and the difference in the average non-bonded energy ΔE_{nb} relative to the maximum value (bottom panel) of the solvated and charge neutralized PONs Models listed in Fig. 4 after *NPT* equilibration, and shown in color (or hues in print) as noted in the legend.

Experimental evaluation of HEG-PONs coverage on a flat, polycrystalline Au surface

XPS analysis was used to compare the coverage of aliphatic-terminated PONs ligands with different degrees of amination on flat, polycrystalline Au surfaces. In a previous study [31] where we used PONs as a model polymeric ligand to investigate how amine content impacts the strength of PONs-AuNP interactions with unilamellar liposomes a combination of XPS and TGA was used to show that reactions between HEG-modified Au NPs and PONs lead to EDC coupling. As shown in Fig. 11 and consistent with this covalent coupling of PONs to the Au NPs, the Au 4f signal was significantly attenuated in samples functionalized with PON-50, PON-55, PON-75, and PON-95, indicating that the PONs ligands with 50-95% amine chain content conjugated to the HEG spacer and covered the Au substrate. There was no significant impact of amination density in this 50-95% range. However, once the amine side chain content reached 100% (PON-100), there was no measurable attenuation of the Au substrate signal, indicating that only minimal conjugation to the HEG spacer was achieved when all side chains were aminated. Thus, a markedly different surface coverage of the PON-100 was observed compared to all other PONs amination densities studied.

These experimental results corroborate the computational models which showed that for PONs with aliphatic side chains, PON-50 was more stable than PON-100. These results are also supported by previous work examining PON-50 versus PON-100 coverage on the same type of Au surfaces, which showed 2-5 times greater conjugation of PON-50.[31]

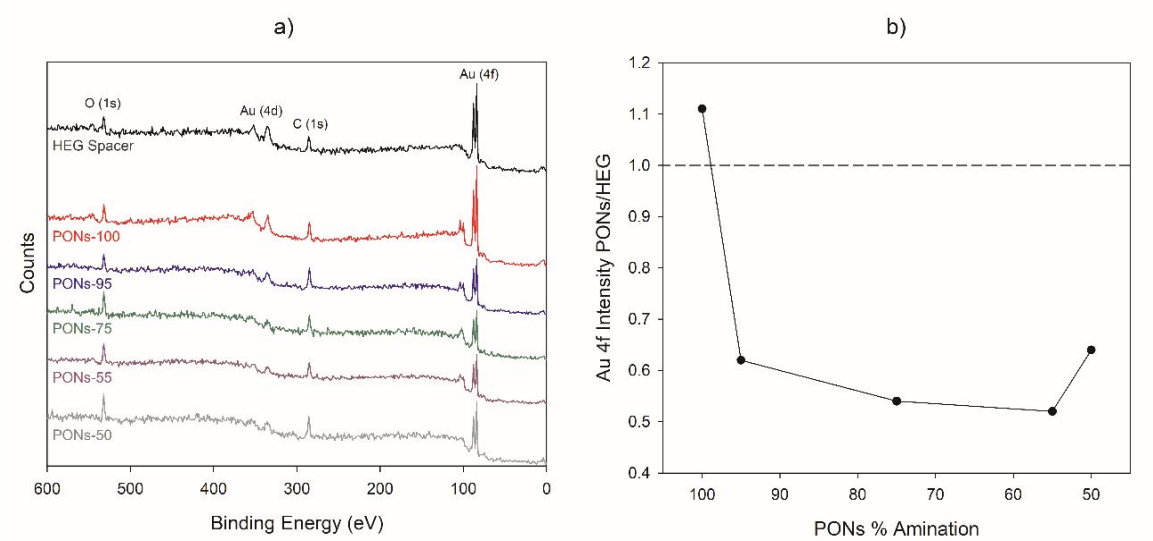

Figure 11. a) XPS survey spectra after Au substrates were functionalized with a HEG spacer and PONs with different degrees of amination, b) Au 4f intensity for samples functionalized with PONs conjugated to HEG spacer normalized to Au substrate functionalized with HEG spacer alone.

In the solution conditions used for the EDC coupling, where HEPES buffer was used to maintain a pH of 6.0, the aminated side chains of the PONs ligands can be expected to be positively charged as shown in Fig. 2c-d. Computational results for the charged aliphatic model showed slightly more stability for mixtures of PON-50 and PON-100 than for either PONs type examined independently (Fig. 10). Experimental results also showed a minor increase in conjugation for PON-55, PON-75, and PON-95 when compared to PON-50 or PON-100, but this was much less significant than the difference in conjugation behavior between PON-100 and all other PONs structures. While the intermediate PON-55, PON-75, and PON-95 structures studied experimentally are not structurally identical to the mixtures of PON-50 and PON-100 molecules studied computationally, they represent the same ranges of differences in the total amine contents within the total area of PONs coverages. In the computed configurations shown in Fig. 4, the global amine side chain content of the mixtures ranges from 56% (eight PON-50 and one PON-100 molecules) to 94% (one PON-50 and eight PON-100 molecules), and therefore explore the same 55-95% amination range studied in the experimental work. There is, however a difference resulting from the fact that each of the copolymers in the experimental work contained a narrower distribution of aminated groups centered at the overall composition rather than the bimodal distribution in the simulations. This difference in the partitioning of the amine side chains could lead to differences in the mixing of the strands. These differences are smaller at the intermediate amine densities when both the experimental results and computational models revealed a slight increase in PONs coverage. It may also be the origin for the primary effect observed in the

experimental work in which the PONs coverage dropped significantly from PON-95 to PON100. As all the chains in the experiment are co-polymers for the PON-*x* cases in which *x* is less than 100%, there is a dramatic change in the structures in going from all-PON95 to all-PON-100 which can account for an emergent deviation in their self-assembly.

While Zheng *et al*.[31] did not examine PON conjugation for the intermediate (55-95%) aminations, the greater coverage achieved for the PON-50 over the PON-100 was associated with greater membrane disruption activity, as shown in their Fig. 11. Specifically, the study showed that liposome lysis efficiency was greatest when cells were exposed to AuNPs coated with PON-50, and then systematically decreased as PONs amination increased until it was completely mitigated for PON-95 and PON-100.[31] This behavior was hypothesized to be due to a gradient of decreasing PONs coverage as amination increased, but in this study it was observed that only PON-100 had significantly decreased coverage. Therefore, the systematic decrease in liposome disruption from PON-50 to PON-95 is likely to be influenced by other changes to particle characteristics, including the reported decreases in ζ-potential and potential changes to overall particle hydrophobicity.[31]

Conclusions

Using a combination of computational and experimental techniques, we have determined molecular and structural properties of PONs conjugated to gold nanoparticle surfaces as these are both key factors in determining biological toxicity.

Through molecular dynamics simulation, we observe the detailed structure of a single (or free) HEG-PONs on the surface of gold nanoparticles with varying diameters in comparison to a planar surface. The effective footprint of the HEG-PONs decreases with increasing curvature and leads to decreased interaction between the NP surface and amines on a given HEG-PONs. The observed footprint of the collapsed free HEG-PONs on the planar surface was seen to be greater than the corresponding distance between the HEG-PONs reported earlier, thus verifying that those particles were at a density at which the chains are interacting.

Assemblies of HEG-PONs on a gold surface were constructed computationally in order to determine the relative stability of mixtures of PONs with varying amine content. We found that assemblies that include a higher percentage of aliphatic PON-50 (that is, PONs for which 50% terminal groups are aliphatic amines), are increasingly more energetically stable than assemblies with all PON-100. Thus, our statistical interaction energy analysis provides a possible molecular origin to experimentally observed behaviors in PON conjugation with varying amine content and composition: higher conjugation efficiency of PON-50 and the collapsing behavior of PON-100. Namely, the increased amine content drives the chains to collapse with a larger number of amine to surface contacts, leading to a decreased number of sections of neighboring PONs available to conjugate.

We also constructed computational assemblies of aromatic HEG-PONs on a gold surface although they have not been synthesized to our knowledge. We found that they have high energetic stability despite their high amine content. Specifically, replacing aliphatic amine terminal groups with aromatic amine terminal groups in PON-50, resulting in more energetically stable configurations with increasing aromatic content in PON-100. However, it is possible that such

structures might collapse in practice due to their hydrophobicity. This suggests that aromatic HEG-PONs may be an interesting target for experimental synthesis and application.

ACKNOWLEDGMENTS

We thank Dr. Karen Lienkamp for many fruitful discussions. This work was supported by National Science Foundation under the Center for Sustainable Nanotechnology (CSN), CHE-1503408. The CSN is part of the Centers for Chemical Innovation Program. Computing resources were provided in part by the National Science Foundation through XSEDE resources under grant number CTS090079 and by the Maryland Advanced Research Computing Center (MARCC).

REFERENCES:

1. Sun, T.; Zhang, Y. S.; Pang, B.; Hyun, D. C.; Yang, M.; Xia, Y. Engineered Nanoparticles for Drug Delivery in Cancer Therapy. *Angew. Chem. Int. Ed.* **2014,** *53*, 12320-12364.
2. Roco, M. C. The Long View of Nanotechnology Development: The National Nanotechnology Initiative at 10 years. *J. Nanopart. Res* **2011,** *13*, 427-445.
3. Bogart, L. K.; Pourroy, G.; Murphy, C. J.; Puntes, V.; Pellegrino, T.; Rosenblum, D.; Peer, D.; Lévy, R., Nanoparticles for Imaging, Sensing, and Therapeutic Intervention. ACS Nano: 2014; Vol. 8, pp 3107-22.
4. Murphy, C. J.; Vartanian, A. M.; Geiger, F. M.; Hamers, R. J.; Pedersen, J. A.; Cui, Q.; Haynes, C. L.; Carlson, E. E.; Hernandez, R.; Klaper, R. D., et al. Biological Responses to Engineered Nanomaterials: Needs for the Next Decade. *ACS Cent. Sci.* **2015,** *1*, 117–123.
5. Cui, Q.; Hernandez, R.; Mason, S. E.; Frauenheim, T.; Pedersen, J. A.; Geiger, F. Sustainable Nanotechnology: Opportunities and Challenges for Theoretical/Computational Studies. *J. Phys. Chem. B* **2016,** *120*, 7297-7306.
6. Mahdavian, A. R.; Mirrahimi, M. A.-S. Efficient Separation of Heavy Metal Cations by Anchoring Polyacrylic Acid on Superparamagnetic Magnetite Nanoparticles through Surface Modification. *Chem. Eng. J.* **2010,** *159*, 264-271.
7. Sperling, R. A.; Parak, W. J. Surface Modification, Functionalization and Bioconjugation of Colloidal Inorganic Nanoparticles. *Philos. Trans. A. Math. Phys. Eng. Sci.* **2010,** *368*, 1333-1383.
8. Kango, S.; Kalia, S.; Celli, A.; Njuguna, J.; Habibi, Y.; Kumar, R. Surface Modification of Inorganic Nanoparticles for Development of Organic–Inorganic Nanocomposites—a Review. *Prog. Polym. Sci.* **2013,** *38*, 1232-1261.
9. Bozich, J. S.; Lohse, S. E.; Torelli, M. D.; Murphy, C. J.; Hamers, R. J.; Klaper, R. D. Surface Chemistry, Charge and Ligand Type Impact the Toxicity of Gold Nanoparticles to Daphnia Magna. *Environ. Sci.: Nano.* **2014,** *1*, 260-270.
10. Salatin, S.; Maleki Dizaj, S.; Yari Khosroushahi, A. Effect of the Surface Modification, Size, and Shape on Cellular Uptake of Nanoparticles. *Cell. Biol. Int.* **2015,** *39*, 881-890.
11. Chen, Y.; Xianyu, Y.; Jiang, X. Surface Modification of Gold Nanoparticles with Small Molecules for Biochemical Analysis. *Acc. Chem. Res.* **2017,** *50*, 310-319.

12. Lee, H.; Lee, E.; Kim, D. K.; Jang, N. K.; Jeong, Y. Y.; Jon, S. Antibiofouling Polymer-Coated Superparamagnetic Iron Oxide Nanoparticles as Potential Magnetic Resonance Contrast Agents for in Vivo Cancer Imaging. *J. Am. Chem. Soc.* **2006,** *128*, 7383-7389.
13. Kim, D.; Park, S.; Lee, J. H.; Jeong, Y. Y.; Jon, S. Antibiofouling Polymer-Coated Gold Nanoparticles as a Contrast Agent for in Vivo X-Ray Computed Tomography Imaging. *J. Am. Chem. Soc.* **2007,** *129*, 7661-7665.
14. Ojea-Jiménez, I.; García-Fernández, L.; Lorenzo, J.; Puntes, V. F. Facile Preparation of Cationic Gold Nanoparticle-Bioconjugates for Cell Penetration and Nuclear Targeting. *ACS Nano* **2012,** *6*, 7692-7702.
15. Milano, G.; Santangelo, G.; Ragone, F.; Cavallo, L.; Di Matteo, A. Gold Nanoparticle/Polymer Interfaces: All Atom Structures from Molecular Dynamics Simulations. *J. Phys. Chem. C* **2011,** *115*, 15154-15163.
16. Stahlhofen, W.; Rudolf, G.; James, A. C. Intercomparison of Experimental Regional Aerosol Deposition Data. *Journal of Aerosol Medicine* **1989,** *2*, 285-308.
17. Lam, C.-W.; James, J. T.; McCluskey, R.; Hunter, R. L. Pulmonary Toxicity of Single-Wall Carbon Nanotubes in Mice 7 and 90 Days after Intratracheal Instillation. *Toxicol. Sci.* **2004,** *77*, 126-134.
18. Roco, M. C., Environmentally Responsible Development of Nanotechnology. *Environ. Sci. Technol*: 2005; Vol. 39, pp 106A-112A.
19. Lee, K. J.; Nallathamby, P. D.; Browning, L. M.; Osgood, C. J.; Xu, X.-H. N. In Vivo Imaging of Transport and Biocompatibility of Single Silver Nanoparticles in Early Development of Zebrafish Embryos. *ACS Nano* **2007,** *1*, 133-143.
20. Ray, P. C.; Yu, H.; Fu, P. P. Toxicity and Environmental Risks of Nanomaterials: Challenges and Future Needs. *J Environ Sci Health C Environ Carcinog Ecotoxicol Rev* **2009,** *27*, 1-35.
21. Taghavi, S. M.; Momenpour, M.; Azarian, M.; Ahmadian, M.; Souri, F.; Taghavi, S. A.; Sadeghain, M.; Karchani, M. Effects of Nanoparticles on the Environment and Outdoor Workplaces. *Electron Physician* **2013,** *5*, 706-712.
22. Tlili, A.; Cornut, J.; Behra, R.; Gil-Allué, C.; Gessner, M. O. Harmful Effects of Silver Nanoparticles on a Complex Detrital Model System. *Nanotoxicology* **2016,** *10*, 728-735.
23. Goodman, C. M.; McCusker, C. D.; Yilmaz, T.; Rotello, V. M. Toxicity of Gold Nanoparticles Functionalized with Cationic and Anionic Side Chains. *Bioconjug. Chem.* **2004,** *15*, 897-900.
24. Arnida; Malugin, A.; Ghandehari, H. Cellular Uptake and Toxicity of Gold Nanoparticles in Prostate Cancer Cells: A Comparative Study of Rods and Spheres. *J. Appl. Toxicol.* **2010,** *30*, 212-217.
25. Feng, Z. V.; Gunsolus, I. L.; Qiu, T. A.; Hurley, K. R.; Nyberg, L. H.; Frew, H.; Johnson, K. P.; Vartanian, A. M.; Jacob, L. M.; Lohse, S. E., et al. Impacts of Gold Nanoparticle Charge and Ligand Type on Surface Binding and Toxicity to Gram-Negative and Gram-Positive Bacteria. *Chem. Sci.* **2015,** *6*, 5186-5196.
26. Hühn, D.; Kantner, K.; Geidel, C.; Brandholt, S.; De Cock, I.; Soenen, S. J. H.; Rivera_Gil, P.; Montenegro, J.-M.; Braeckmans, K.; Müllen, K., et al. Polymer-Coated Nanoparticles Interacting with Proteins and Cells: Focusing on the Sign of the Net Charge. *ACS Nano* **2013,** *7*, 3253-3263.
27. Sunshine, J. C.; Peng, D. Y.; Green, J. J. Uptake and Transfection with Polymeric Nanoparticles Are Dependent on Polymer End-Group Structure, but Largely Independent of Nanoparticle Physical and Chemical Properties. *Mol. Pharm.* **2012,** *9*, 3375-3383.

28. Su, C.-F.; Merlitz, H.; Rabbel, H.; Sommer, J.-U. Nanoparticles of Various Degrees of Hydrophobicity Interacting with Lipid Membranes. *J. Phys. Chem. Lett.* **2017,** *8*, 4069-4076.
29. Timofeeva, L.; Kleshcheva, N. Antimicrobial Polymers: Mechanism of Action, Factors of Activity, and Applications. *Appl. Microbiol. Biotechnol.* **2011,** *89*, 475-492.
30. Lienkamp, K.; Madkour, A. E.; Musante, A.; Nelson, C. F.; Nüsslein, K.; Tew, G. N. Antimicrobial Polymers Prepared by Romp with Unprecedented Selectivity: A Molecular Construction Kit Approach. *J. Am. Chem. Soc.* **2008,** *130*, 9836-9843.
31. Zheng, Z.; Saar, J.; Zhi, B.; Qiu, T. A.; Gallagher, M. J.; Fairbrother, D. H.; Haynes, C. L.; Lienkamp, K.; Rosenzweig, Z. Structure–Property Relationships of Amine-Rich and Membrane-Disruptive Poly(Oxonorbornene)-Coated Gold Nanoparticles. *Langmuir* **2018,** *34*, 4614-4625.
32. Brown, W. M.; Wang, P.; Plimpton, S. J.; Tharrington, A. N. Implementing Molecular Dynamics on Hybrid High Performance Computers–Short Range Forces. *Comput. Phy. Comm.* **2011,** *182*, 898-911.
33. Nelson, M. T.; Humphrey, W.; Gursoy, A.; Dalke, A.; Kalé, L. V.; Skeel, R. D.; Schulten, K. Namd: A Parallel, Object-Oriented Molecular Dynamics Program. *J. Supercomputing. App.* **1996,** *10*, 251-268.
34. Vanommeslaeghe, K.; Hatcher, E.; Acharya, C.; Kundu, S.; Zhong, S.; Shim, J.; Darian, E.; Guvench, O.; Lopes, P.; Vorobyov, I. CHARMM General Force Field: A Force Field for Drug-Like Molecules Compatible with the CHARMM All-Atom Additive Biological Force Fields. *J. Comput. Chem.* **2010,** *31*, 671-690.
35. Robertson, M. J.; Tirado-Rives, J.; Jorgensen, W. L. Performance of Protein-Ligand Force Fields for the Flavodoxin-Flavin Mononucleotide System. *J. Phys. Chem. Lett.* **2016,** *7*, 3032-3036.
36. Lienkamp, K.; Kumar, K.-N.; Som, A.; Nüsslein, K.; Tew, G. N. "Doubly Selective" Antimicrobial Polymers: How Do They Differentiate between Bacteria? *Chemistry* **2009,** *15*, 11710-11714.
37. Bartczak, D.; Kanaras, A. G. Preparation of Peptide-Functionalized Gold Nanoparticles Using One Pot Edc/Sulfo-Nhs Coupling. *Langmuir* **2011,** *27*, 10119-10123.

Table of Content Graphic

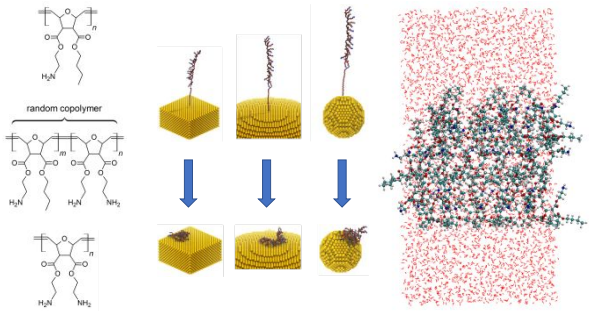

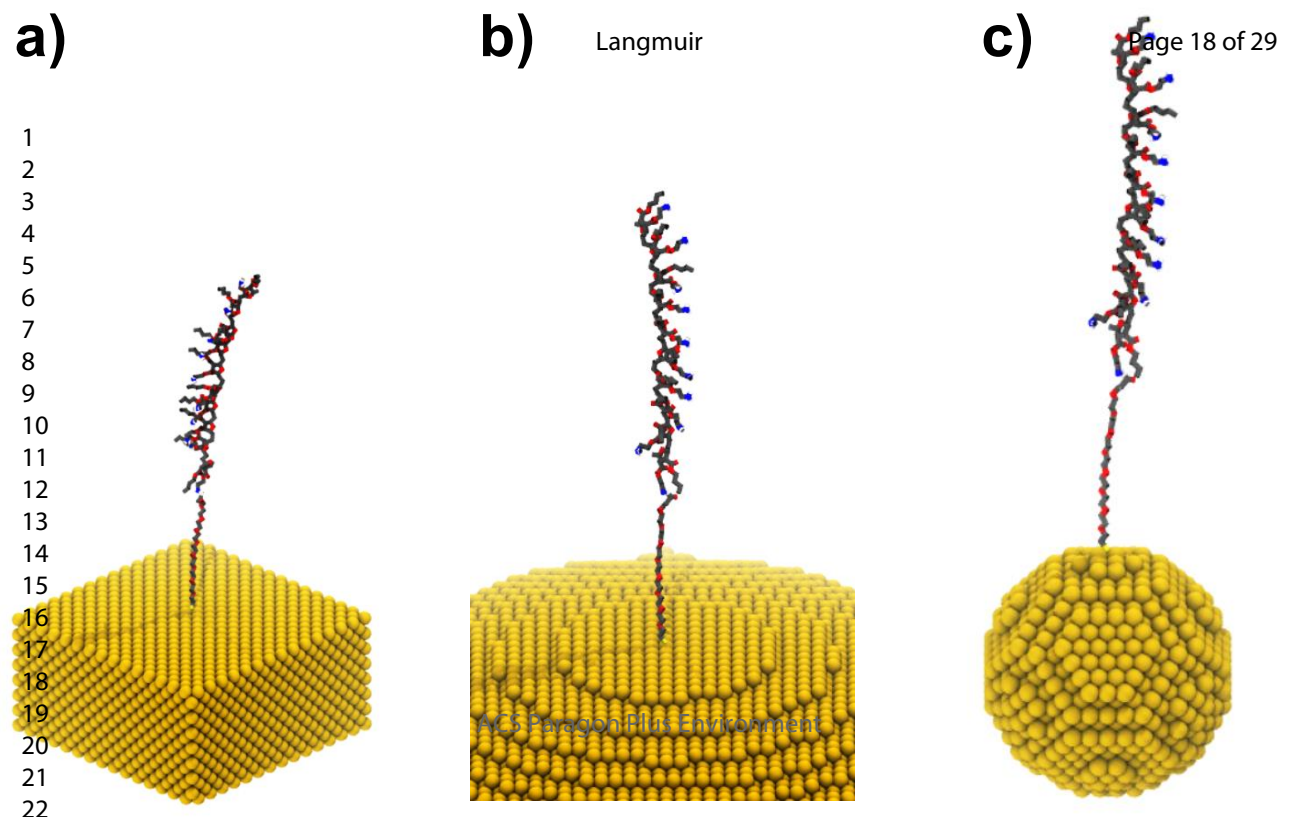

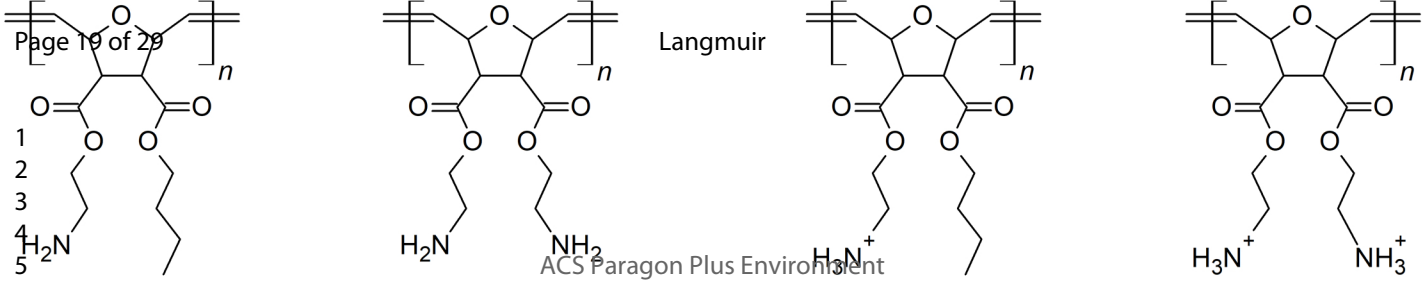

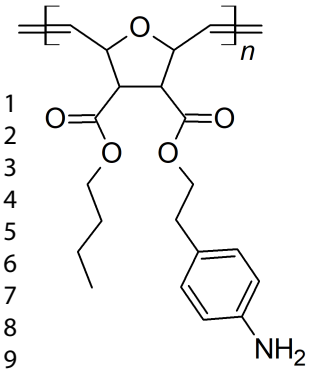

a)

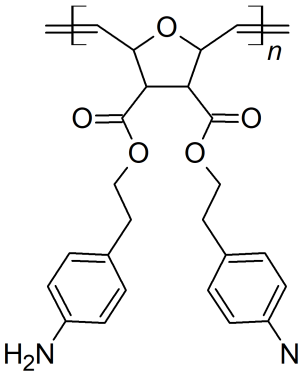

b)

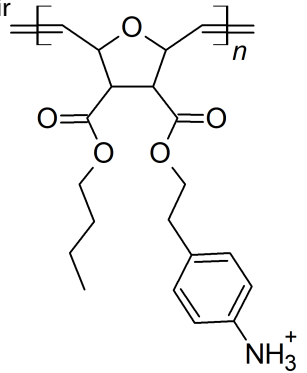

c)

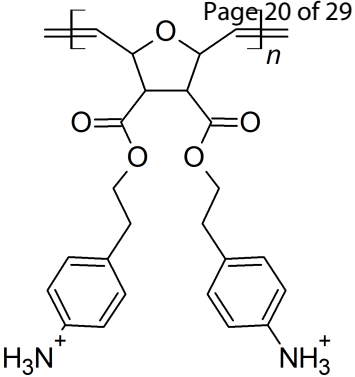

d)

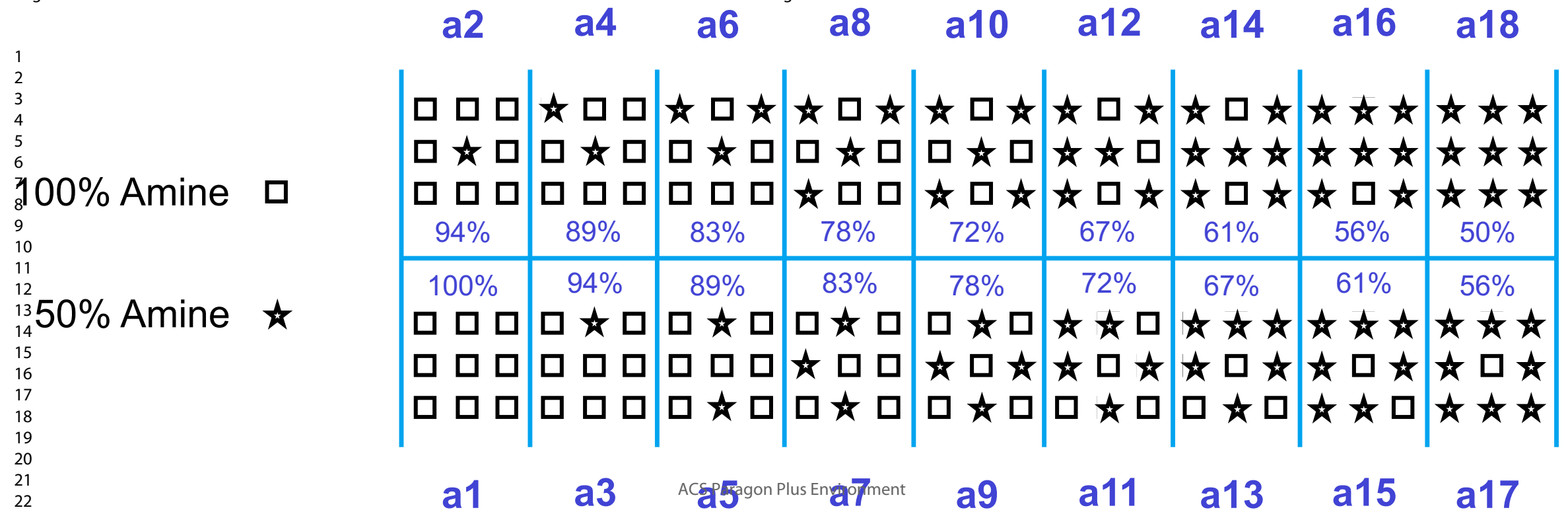

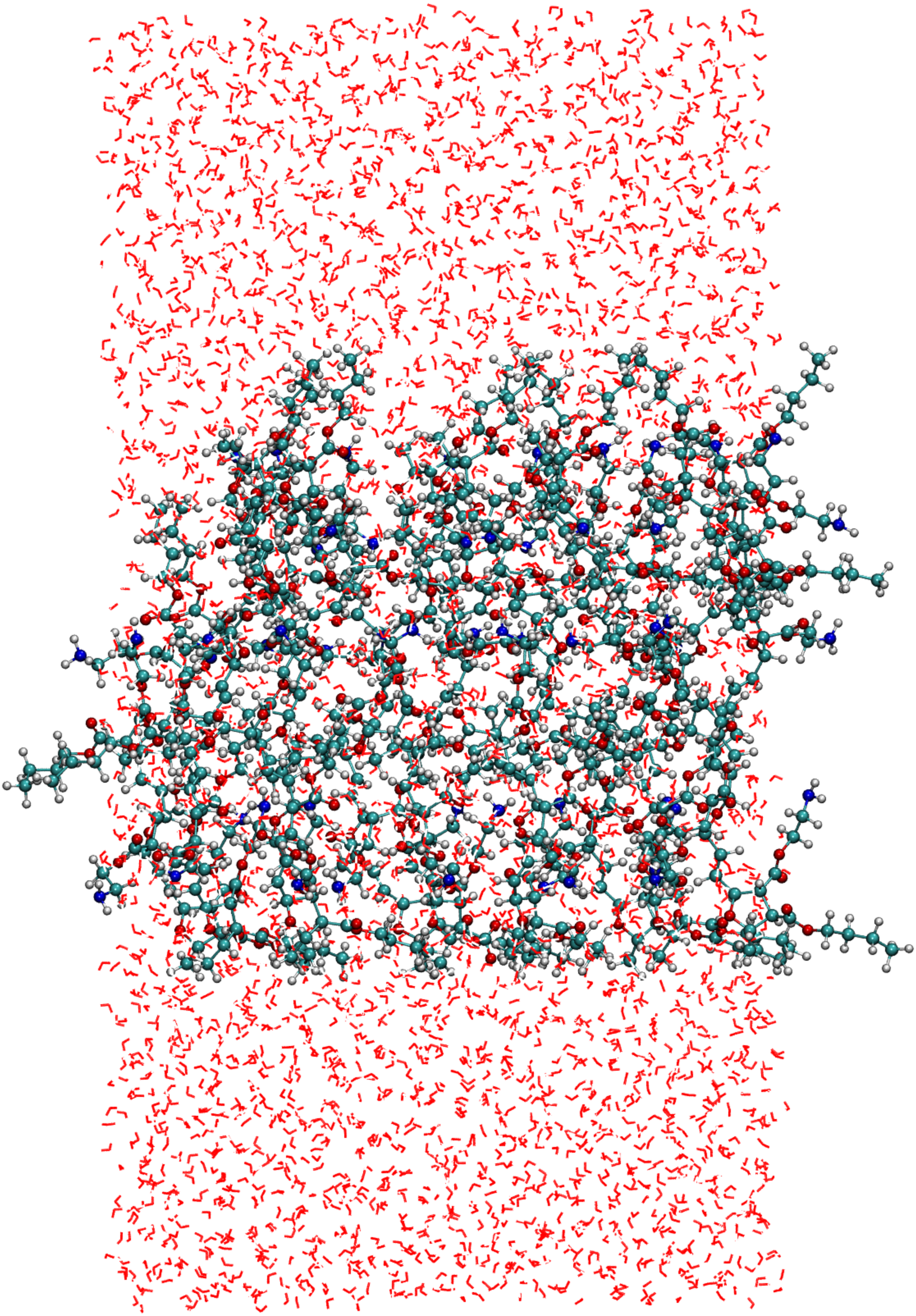

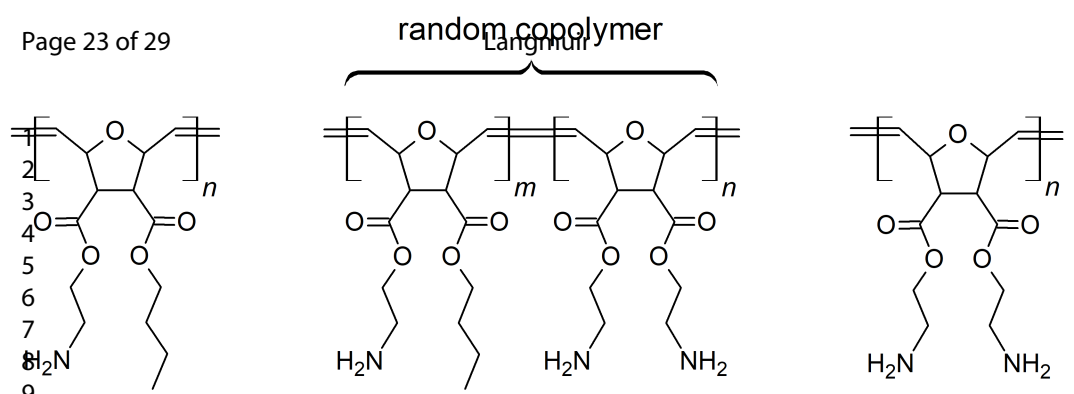

a)

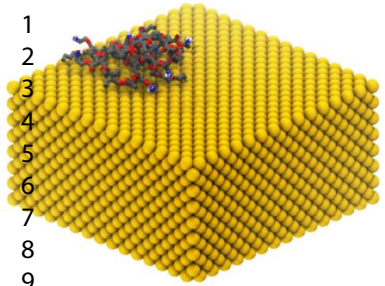

b)

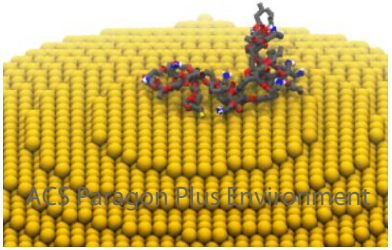

c)

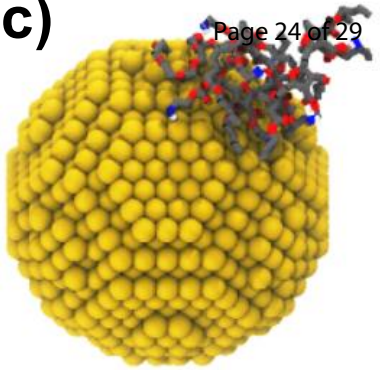

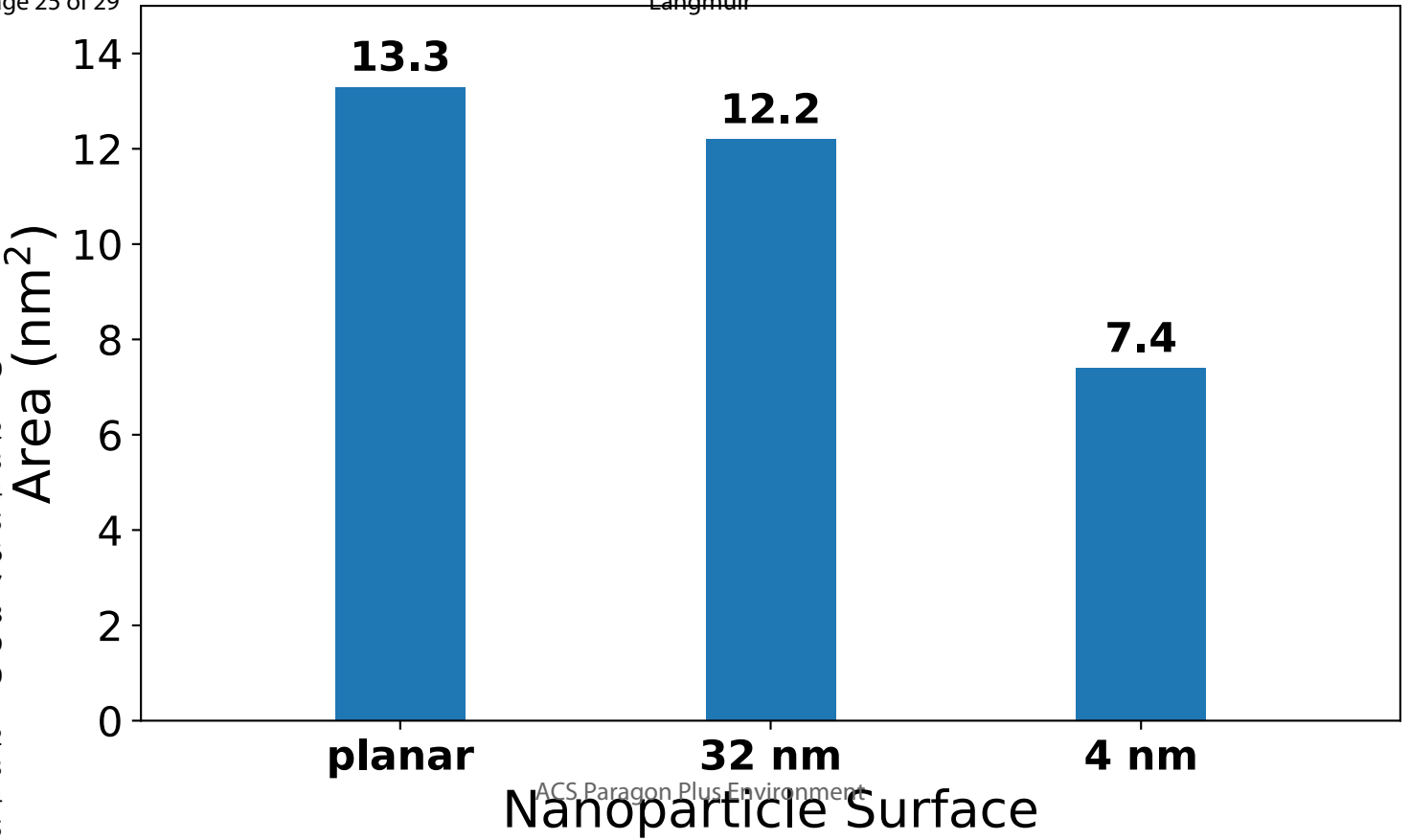

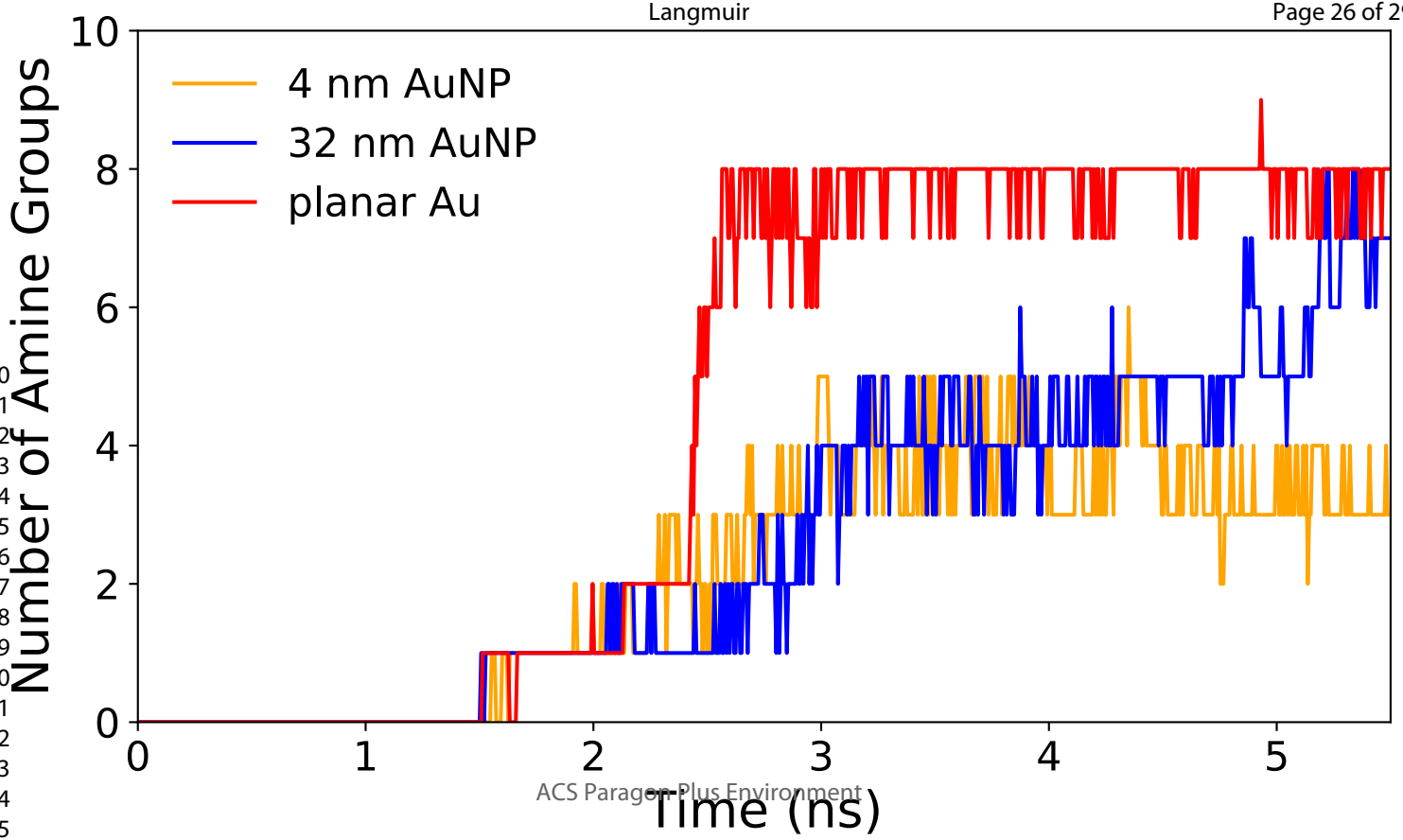

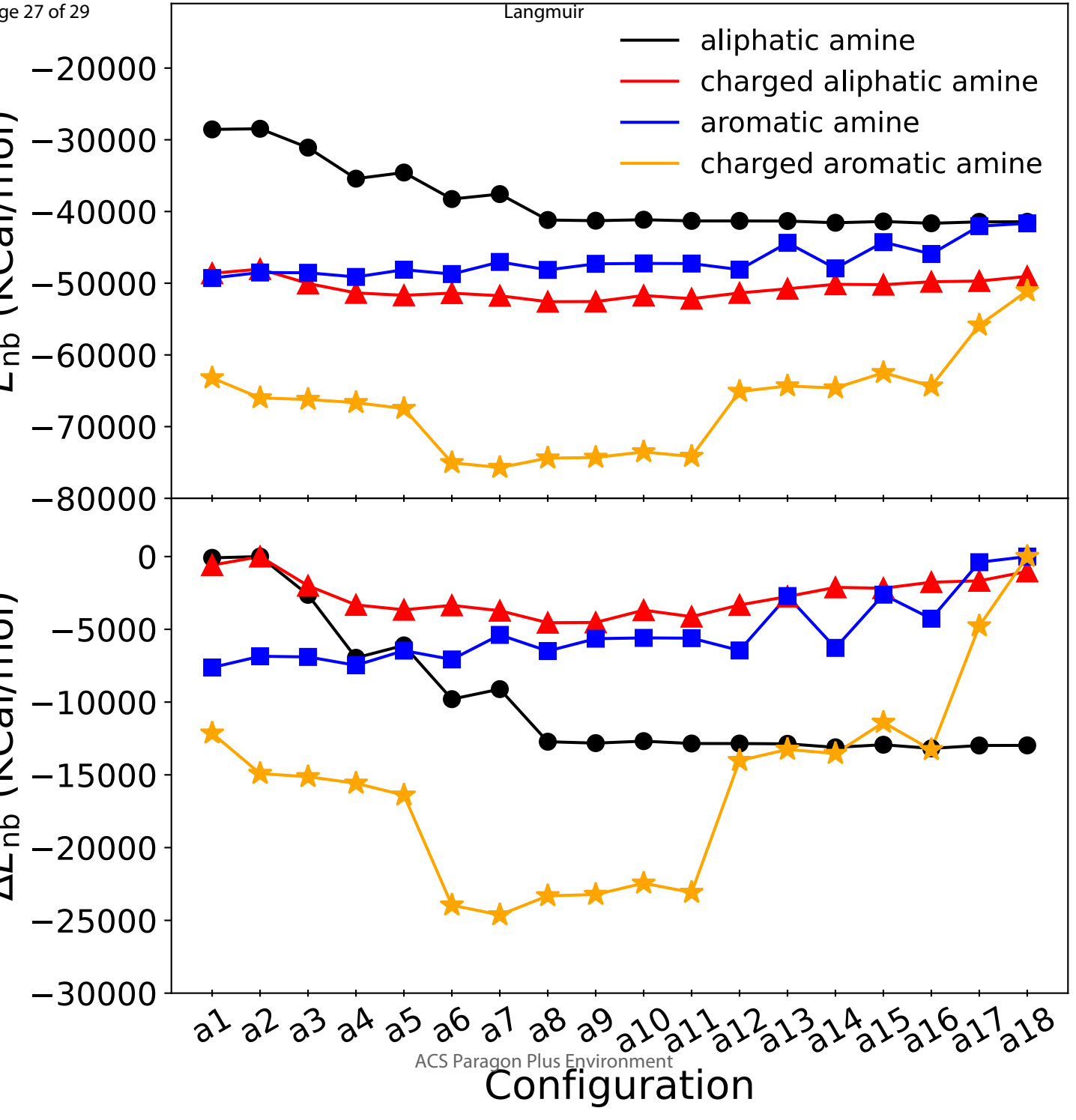
aliphatic amine
charged aliphatic amine
aromatic amine
charged aromatic amine
E_{nb} (KCal/mol)
ΔE_{nb} (KCal/mol)
−20000
−30000
−40000
−50000
−60000
−70000
−80000
0
−5000
−10000
−15000
−20000
−25000
−30000
a1 a2 a3 a4 a5 a6 a7 a8 a9 a10 a11 a12 a13 a14 a15 a16 a17 a18
Configuration

a)

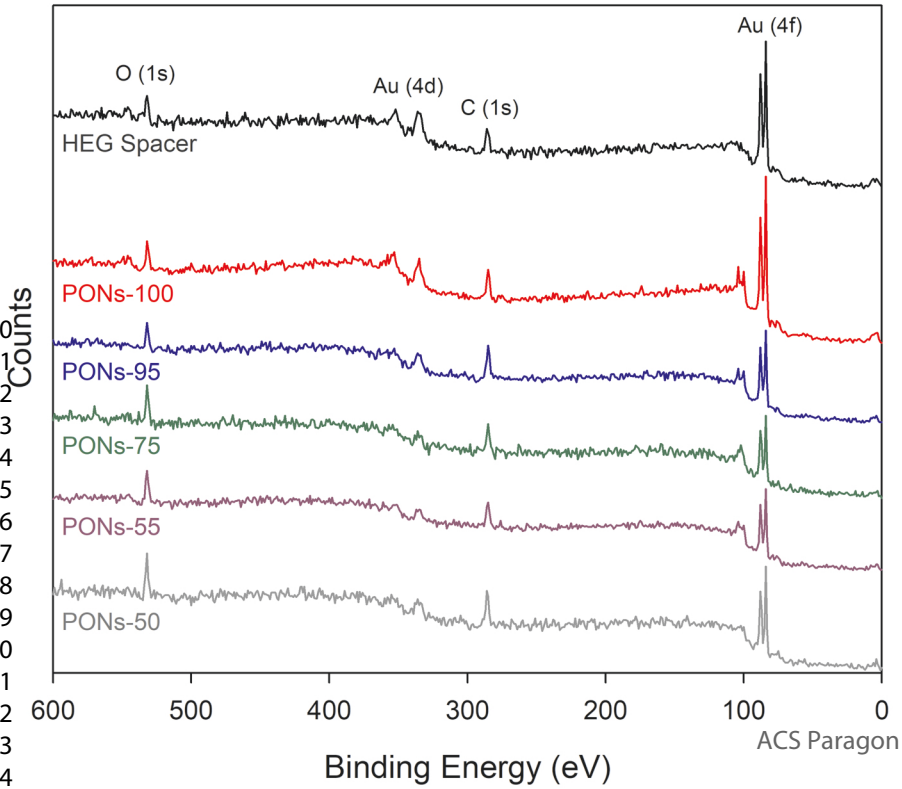
Au (4f)
O (1s)
Au (4d)
C (1s)
HEG Spacer
PONs-100
PONs-95
PONs-75
PONs-55
PONs-50
Counts
600
500
400
300
200
100
0
Binding Energy (eV)

b)

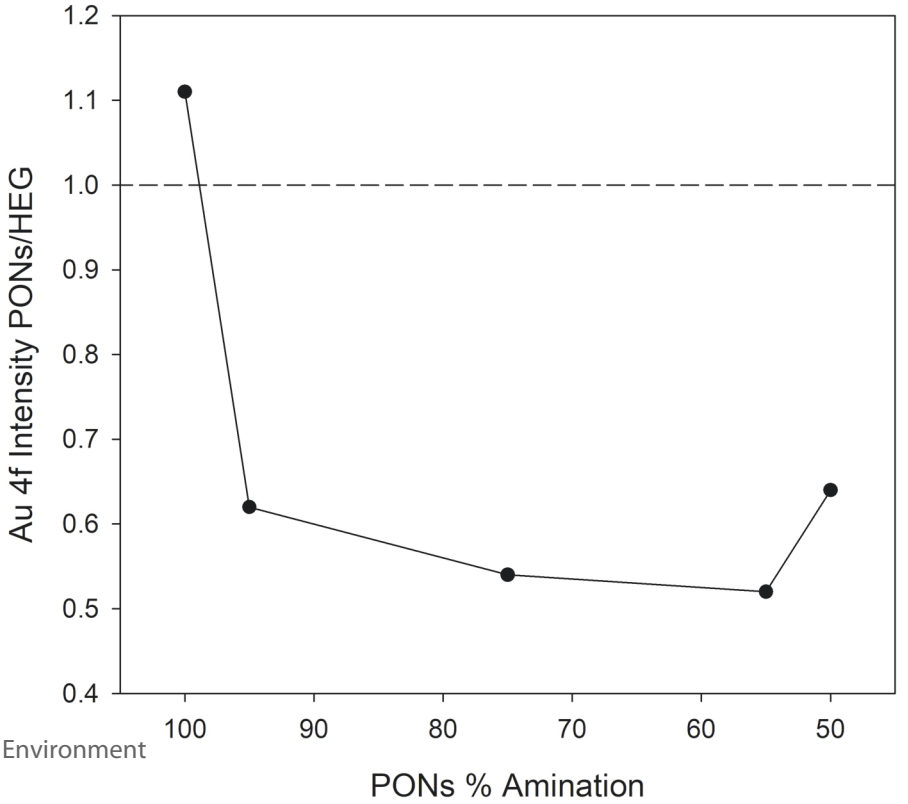
1.2
1.1
1.0
0.9
0.8
0.7
0.6
0.5
0.4
Au 4f Intensity PONs/HEG
100
90
80
70
60
50
PONs % Amination

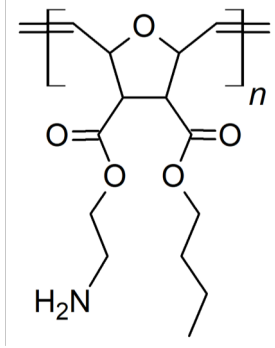

random copolymer